Arch. Metall. Mater. **71** (2026), 1, 133-150

DOI: https://doi.org/10.24425/amm.2026.157776

SIVAGANESAN VEMBAR[1*], MATHALAI SUNDARAM CHANDRASEKAR[1]

PERFORMANCE OPTIMIZATION ON SQUEEZE CASTING PROCESS PARAMETERS OF AA7075 BASED COMPOSITES FOR CORROSIVE ENVIRONMENT

Aluminium Hybrid Metal-Matrix Composites (AHMMCs) are advanced materials used in lightweight, high-strength applications, notably in aerospace and automotive industries. This study utilized AA7075 for its strength and ductility, improving its wear and corrosion resistance by reinforcing it with 12 wt.% titanium carbide (TiC) and varying amounts (2-6 wt.%) of boron nitride (BN) using squeeze casting. Process parameters-melting temperature, squeeze pressure, and period of stirring are optimized using Design Matrix of L9 and Grey Relational Method (GRM), with 750°C, 100 MPa, 15 minutes, and 4 wt.% BN identified as optimal. SEM analysis confirmed uniform BN distribution up to 4 wt.%, while 6 wt.% led to agglomeration due to weak wetting and high surface-energy. Mechanical and corrosion properties were significantly improved with 4 wt.% BN, including increases in microhardness (68%), tensile strength (29.6%), compressive strength (29.5%), impact strength (87%), wear resistance (69%), and corrosion resistance (64.5%) compared to unreinforced AA7075. These enhancements are attributed to refined microstructure, better load transfer, and improved resistance to dislocation and surface degradation. The study confirms the potential of BN and TiC-reinforced AA7075 composites for high-performance engineering applications.

Keywords: Aluminium alloy 7075; Titanium Carbide; Boron Nitride; Squeeze casting; Mechanical properties; Tribological properties

1. Introduction

Composite properties can be improved by refining matrix grains and particle sizes. Conventional metal matrix composites should have greater microstructural stability and better mechanical properties than nano crystalline matrices with nanoscale reinforcement [1]. The stir casting technique was employed to study how different weight percentages (0%, 3%, 5%, and 7%) of nano aluminum oxide (Al_2O_3, particle size less than 100 nm) affected the mechanical, wear and microstructural behaviors of Al7075 metal-reinforced composites. Findings showed a positive correlation between nanoparticle content and mechanical attributes, up to a point, with a subsequent decrease observed at 7% nanoparticle loading [2]. Wear characteristics of Al7075 AMMCs, fortified with different propositions of Al_2O_3 and Gr particulates, were evaluated during sliding tests (dry) using a pin-disc tribometer experiment. The experimental trials were structured and carried out according to the orthogonal array strategy of the Taguchi technique [3]. A composite material was produced using a two-stage stir casting method, incorporating silicon carbide and titanium carbide particles in volume fractions ranging from 5% to 15%. To evaluate wear and friction characteristics, sliding tests (dry) was performed using a pin-disc tribometer experiment at ambient temperature, without lubrication. Experimented the sliding test with applied loads of 10, 20, and 30 N, used the speeds of 1, 2, and 3 m/s correspondingly. Results indicated that titanium carbide-reinforced composites exhibited 18.8% higher microhardness than those reinforced with silicon carbide [4]. Wear rate analysis revealed that titanium carbide composites, 2.1×10^{-3} mm^3/m wear rate, whereas silicon carbide composites exhibited a wear of 6.4×10^{-3} mm^3/m. Additionally, an increase of load and sliding velocity led to a higher wear rate [5]. The reinforcement of TiC particles with 2.5 wt.% and 5 wt.% to the AA7075 composites were examined for their microstructure, hardness, wear, and corrosion behavior. Upon adding TiC to AA7075, a transition from a prominent dendritic structure to a non-dendritic one was observed through microscopy. The presence of TiC also triggered the precipitation of secondary phases, including Al_2CuMg, Al_2Cu, and Fe-rich phases Al_7Cu_2Fe and $Al_6(Cu,Fe)$, in both inter- and intra-dendritic zones. This strengthening, attributed to grain boundary and particle mechanisms, resulted in higher composite hardness. Notably, an opposite trend was seen between TiC con-

[1] DEPARTMENT OF MECHANICAL ENGINEERING, NADAR SARASWATHI COLLEGE OF ENGINEERING AND TECHNOLOGY, THENI, TAMIL NADU INDIA

* Corresponding author: sivaganesan8686@gmail.com

centration and both the friction coefficient and wear rate [6]. AA 7075 composites with 12 wt.% boron nitride (BN) demonstrated a minimum density (2.70 g/cm^3). The mechanical attributes of these composites were notably enhanced, with the 12 wt% BN composition achieved the tensile strength maximum of 210 MPa. The enhancement of tensile strength of 26% was achieved by adding of 4 wt.% BN in the AA 7075 matrix. Microscopic evaluation of the worn surfaces showed plough formations within the AA 7075–4 wt.% BN composite. The furrow formations within the AA 7075 addition of 8 (wt.%) BN composite [7]. These alloys can be formed using diverse manufacturing procedures. Casting is a particularly uncomplicated and budget-friendly option. Nevertheless, components produced through casting are frequently vulnerable to defects such as porosity, gas inclusions, and contraction issues, all of which originate during the casting operation [8]. Squeeze casting was created as a means of reducing the flaws associated with standard casting procedures. This method integrates pouring with a compressive step, essentially a forging action. The pressure exerted after the molten metal is introduced into the die is a primary determinant of the final part's soundness. Furthermore, the characteristics of the manufactured piece are greatly affected by the melting point, compression interval, and mould heating temperature [9]. Melt temperature, compression pressure, and time affect alloy mechanical and wear properties. Changes in these parameters, especially compression pressure, melt temperature, and mold preheat, significantly impact alloy characteristics, improving strength, grain structure, and wear resistance [10]. Alloying improves mechanical strength of AA7075, but its corrosion resistance is low due to electrochemical differences between particles and the matrix. Zinc and magnesium intermetallics act as anodes, making them corrosion prone [11].

There is no research done on the size, dispersion, and chemical makeup of secondary phases show the vital role for finding the hardness, ductility and strength of AA7075 alloy based composites. These phases are vulnerable to localized corrosion, like pitting and intergranular breakdown, due to electrochemical interactions within the base material. While ceramic particles can modify the structural development of secondary phases in AA7075 based composites, further exploration is needed to understand the effects of reinforcements on the alloy's mechanical and Tribological properties under corrosive environment. This research focuses on evaluating the impact of squeeze casting parameters with TiC and BN particle reinforcements on the AA7075 alloy's microstructure, mechanical performance, wear behaviour under NaCl corrosive environments by using GRA.

2. Materials and methods

2.1. Materials

The matrix-material selected for this study is AA7075, a material distinguished by its considerable ductility, elevated strength and superior fatigue performance even though it has moderate tribological and corrosion properties. Nevertheless, compared to many other alloys, AA7075 exhibits a higher tendency towards embrittlement, a consequence of microsegregation [12]. The Aluminum 7075 provided by Trichy Metals, Trichy, India in cylindrical form. Hence, AA7075 is in the need of enhancement of tribological and corrosion properties. The BN and TiC were observed as reinforcement for the enhancement of lacked properties of AA7075. Both reinforcements were purchased with 10 µm and 5 µm in the form of provided by Subra Scientific Company, Chennai, India. Average particle size of Titanium Carbide and Boron Nitride reinforcement particles was confirmed by the Particle Size Analyzer (PSA) [13]. Titanium carbide has exceptional hardness, wear resistance and high melting point make it ideal for demanding aerospace and automotive applications [14]. Boron nitride acts as a heat-resistant lubricant. Both materials exhibit strong resistance to chemicals and extreme temperatures [15]. The compositional analysis of AA7075, TiC and BN is shown in TABLES 1a and 1b. The properties of AA7075, TiC and BN is displayed in TABLE 2.

TABLE 1A

Elements presented in AA7075

Fe	Si	Mn	Cu	Cr	Mg	Ti	Zn	Al
0.24	0.08	0.06	1.5	0.2	2.4	0.07	5.8	Bal.

TABLE 1B

Elements presented in TiC and BN

Element	TiC		BN	
	Ti	C	B	N
Wt.%	72.97	27.03	43.25	56.75

TABLE 2

Properties of Matrix and Reinforcement

Properties	AA7075	BN	TiC
Hardness (VHN)	175	4500	2800
Melting temperature (°C)	635	2973	3160
Density (g/cc)	2.81	3.45	4.93
Poisson's Ratio	0.33	0.21	0.19
Tensile strength (Mpa)	700	400	500

In Fig. 1 the SEM image of Titanium carbide & Boron Nitride is shown and SEM image of TiC reveals that the observed structure is Cubic structure and observed structure for Boron Nitride is Hexagonal. Both structures form higher bonding strength between the matrix and reinforcement materials and it causes to slight enhancement of mechanical and tribological properties. The SEM image of TiC and BN is displayed in 10 µm and 5 µm scale respectively.

2.2. Optimization of process parameters for Squeeze casting

Squeeze casting is the preferable approach for creating AA7075 composites with 12 wt.% TiC and 6 wt.% BN rein-

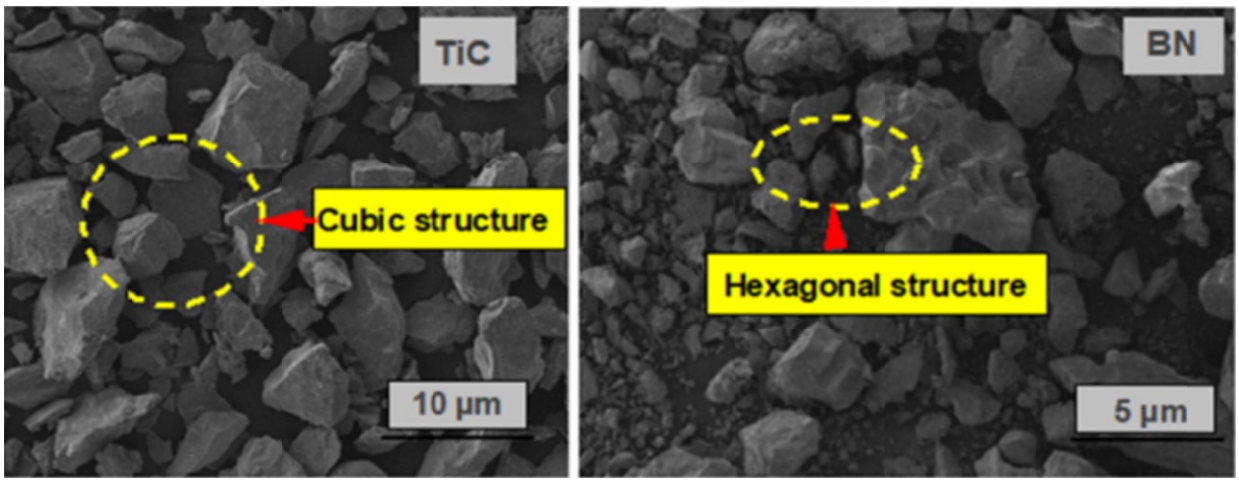

Fig. 1. TiC and BN reinforcements SEM Image

forcements, since it promotes equal reinforcement distribution and reduces porosity. The chosen processing factors have a considerable influence on the quality of the composites produced, particularly their mechanical strength and corrosion behavior. To create AA7075 composites with better mechanical, Tribological and corrosion characteristics, it is important to fine-tune the squeeze casting parameters, highlighting the need of correct process management. The melting temperature (700, 725 and 750°C), Squeeze pressure (50, 75 and 100 MPa), Squeeze time (5,10,15 minutes) and 12 wt.% of TiC + X wt.% BN (X = 2,4 and 6) were selected as input parameters. L9 OA was selected to form the experiments of design and the VHN and UTS were selected as response parameter and the response parameters were evaluated after subjecting into Salt Spray Test (SST) by the usage of KORROX III and the testing procedure consisted of a 120-hour spray application conducted at a pressure of 1.2 kg/cm^2, using a solution with a pH level of 8.2. The salt spray test adhered to ASTM B117 standards. L9 OA displayed in TABLE. 3. Stainless steel crucible was preheated at 850°C and placing of small sized aluminium alloy 7075 cylindrical round was done. Melting of AA7075 in the crucible was based L9 OA formation trials (700, 725 and 750°C). Melted AA7075 was stirred for 10 minutes duration with 700 rpm stirring speed. TiC and BN particle reinforcements were preheated in the muffle furnace (STXMF1896) at 400°C for 30 minutes. Melt stirring, preheated reinforcements and addition of Mg was placed into vortex. In the presence of argon gas flow, stirring of mixture was done for 5 minutes. Stirrer blades were moved downward and upward motion. Pouring of stirred melt in the pre heated die through pre heated runway was done. Applied pressure of 120 MPa after pouring into die for 25 seconds. The same procedure was for followed for fabricating L9 OA based specimens.

Adding 1 wt.% magnesium improved the bonding between the AA7075 matrix and the TiC and BN particles. Preheating the die to 450°C helped prevent cracks, enhanced material flow, and extended the die's lifespan. The die was produced in two dimensions: a cylindrical shape measuring 150 mm in length and 50 mm in diameter, and a plate with dimensions of 150×100×12 mm [16].

The molten mixture of AA7075 with 12 wt.% TiC and varying BN content (2, 4, and 6 wt.%) was then allowed to cool and solidify. Following exposure, hardness test and tensile tests were accomplished to assess microhardness and UTS. All experiments were repeated 3 times, finally the mean datas were recorded. Tensile testing of AA7075 HMMCs followed ASTM E08, with samples prepared by wire EDM. Tensile testing was carried out utilizing a TTSH2000-IUTM machine. As per ASTM E384, the VHN of AA7075 HMMCs was determined using a Metlab-1000 Vicker-Microhardness tester and applied a force 300 g for 15 sec. Vickers Harness tester (ASI- MHVD-1XYZ, MHT 1000DT)) was employed to determine the hardness of L_9 OA based fabricated composites specimens. ASTM E384 was utilized for conducting hardness test. The 3 trials were conducted and mean value has been considered for investigation. SEM with EDAX (HITACHI model S-3000) was employed for to determine the microstructure of fabricated L_9 OA based AA7075 based composites. The abrasive sheets with different grit sizes (600, 900, and 1200) was used for polishing the AA7075 composites for increase the clarity of SEM images and the disparity was further enhanced using Keller's reagent. Porosity was determined

TABLE 3

L9 with input parameters of AA7075/12 wt.% TiC/BN HMMCs

Squeeze Casting Specimen (SCS)	Melting Temperature (°C)	Squeeze Pressure (MPa)	Squeeze Time (minutes)	Stirring speed rpm
SCS1	700	50	5	550
SCS2	700	75	10	600
SC3	700	100	15	650
SCS4	725	50	10	650
SCS5	725	75	15	550
SCS6	725	100	5	600
SCS7	750	50	15	600
SCS8	750	75	5	650
SCS9	750	100	10	550

by determining the bulk density and theoretical density of the L_9 OA based fabricated composites specimens. Bulk density was determined by using Archimedes principle with the help of electronic weighing machine with an accuracy of 0.0001 g (OH30429812 Ohaus Pioneer Precision Balance). Theoretical density of L_9 OA based fabricated composites specimens was calculated based on rules of mixture ($P_{total} = (1-\rho_{th}/\rho_b) \times 100\%$). Minitab 19 was used to perform Taguchi Grey Relational Analysis (GRA) on UTS and VHN. The singe response optimization was reduced from multiresponse optimization using Grey Relational Analysis (GRA), using certain procedural procedures [17]. GRA was implemented by following steps.

Grey relational analysis provides an effective means of optimizing multiple outputs. To effectively analyze numerous process parameters concurrently, bypassing the limitations of standard statistical experiments, this method is widely adopted. Ensuring the precision and consistency of the results necessitates data pre-processing, as diverse goals and situations can lead to inconsistencies. Therefore, response values are scaled to a range of 0 to 1, employing three fundamental normalization strategies: 'minimize the value', 'maximize the value,' and an additional technique.

- Phase-1

  According to the Eq. (1), the data's are normalized based on "larger the better".

$$P_{ab} = \frac{Q_{ab} - \min(Q_{ab})}{\max Q_{ab} - \min(Q_{ab})} \quad (1)$$

  where Q_{ab} are original data for the experimental response a P_{ab} is the pre-processing order following data; minimum Qab was the minimum value of Q_{ab} and maximum Q_{ab} was the largest value of Q_{ab}.

- Phase-2

  According to the Eq. (2), the normalized dada were evaluated using Grey Relational Coefficient (GRC).

$$\left(P_{0b}, P_{ab}\right) = \frac{\Delta_{\min} + \zeta\Delta_{\max}}{\Delta_{ab} + \zeta\Delta_{\max}} \quad (2)$$

  where $\gamma(P_{0b}, P_{ab})$ are the GRC between P_{0b} and P_{ab} and $\zeta = 0.5$.

- Phase-3

  According to the Eq. (3), the GRG was estimated

$$GRG\left(P_{0b}, P_{ab}\right)\sum_{b=1}^{n} P_b \gamma\left(P_{0b}, P_{ab}\right) \quad (3)$$

  where GRG (P_0, P_a) is the grade. P_a is the sequence of comparability and P_0 is sequence of reference. The b is the response weight of P_b and it is depends on the judgement of makers decision. Optimal process parameters correlate with a high gray relational grade. The AA7075/12wt.%TiC/x wt.% BN (0, 2, 4 and 6) HMMCs were fabricated for further testing by using the optimized process parameters of squeeze casting.

2.3. Test of Optimized process parameters based fabricated AA7075 AHMMCs

The optimized squeeze casting process parameter based AA7075 HMMCs were determined based Higher the Better basis on VHN and UTS. The optimization was done by considering calculated GRG. Metallurgical properties such as presence of elements and microstructure of the optimized process parameters based AA7075 HMM composites fabrication were analysed by utilizing EDAX and SEM test. The EDX-SEM Shimadzu system were applied to conducted SEM and EDAX tests. The abrasive sheets with grit sizes of 600, 800, 1000, and 1200 was used for polish the developed test-models to produce 1 μm surface finish [18]. The Surface Roughness Tester (Mitutoyo-SJ210) was used to determine the roughness of the polished AA7075 AHMMCs, measured from 3 trials and mean roughness values are recorded. To improve surface contrast, the Keller's mix was included to the polished AA7075 HMMC [19]. This Keller's mix is a combination of 15% and 5% nitric acid and hydrochloric acid respectively in water. The Archimedes principle was used for measuring the density and porosity which are carried out using for the AA7075 HMMCs based on optimized process parameters fabrication.

The optimized process parameters based fabrication of AA7075 HMMCs were underwent compression, impact, wear and Salt Spray test to find the compressive strength, impact strength, tribological properties after subjecting into Salt Spray Test (SST) by the usage of KORROX III and the testing procedure consisted of a 120-hour spray application conducted with the 1.2 kg/cm^2 pressure, using a solution with a pH level of 8.2 and corrosion resistance respectively [20]. According to the ASTM E09, the compression test was conducted by using of Tinius Olsen H50KL compression test machine on optimized squeeze casting process parameters combination fabricated AA7075 HMMCs [21]. Impact test was conducted on optimized squeeze casting process parameters combination fabricated AA7075 HMMCs by the usage of FIE IT-50as per ASTM D256 [22].Wear test was conducted on optimized squeeze casting process parameters combination fabricated AA7075 HMMCs by the usage of DUCOM – TR 20 – LE at varying applied load of 10, 15, 20, 25 and 30 N with sliding velocity 1.2 m/s and sliding distance 2000 m [23]. Weight was calculated by finding weight of the wear test specimens before and after wear test by the usage of electronic weigh balance ContechCAI-224with an accuracy of 0.0001 g. Friction coefficient was calculated by using frictional force obtained from the wear testing software Nanotech version 3.0. Worn surface and wear debris of better wear test specimens were analysed by using SEM images. The corrosion rate of optimized squeeze casting process parameters combination fabricated AA7075/12wt.%TiC/xwt.%BN (0, 2, 4 and 6) samples was calculated using mass loss method. Further corroded surfaces of these samples were analysed using SEM images.

3. Results and discussion

3.1. Process parameters optimization for Squeeze casting on VHN and UTS by using GRA

TABLE 4 displays the factor information for optimizing the process parameters for Squeeze casting with the use of L9 OA Taguchi design.

TABLE 4

Factors

Factor	Levels	Type	Values
Temperature (Melting) (°C)	3	Fixed	700, 725, 750
Squeeze Pressure (MPa)	3	Fixed	50, 75, 100
Squeeze Time (minutes)	3	Fixed	5, 10, 15
Wt.% of BN	3	Fixed	2, 4, 6

The L9 OA based fabrication of AA7075 AHMMCs were underwent to Vickers Hardness Test and tensile testing and the observed VHN and tensile strength were noted and is shown in TABLE 5. Squeeze casting parameter optimization, the Minitab 19 software was utilized for optimizing the process parameters. For optimization VHN and UTS process parameters of squeeze casting, the Taguchi approach is used.

3.1.1. Hardness due to input process parameters effect

TABLE 6. displays the response table for means of hardness and it reveals that hardness is influenced by the melting temperature, squeeze pressure, squeeze time and wt.% of BN input parameters sequence. Fig. 2 presents the hardness main effect plot, which shows that varied melting temperature between 700 to 750°C in 25°C steps, squeeze pressure from 50 to 100 MPa in 25 MPa steps, and squeeze time from 5 to 15 minutes in 5-minute steps results in an increase in hardness due to increased material densification and reduced porosity. Furthermore, 2 to 4 wt.% of raising of BN, increases hardness because BN works as a reinforcement, improving the composite's mechanical characteristics. However, at 6 wt.% BN, hardness falls due to particle aggregation and weak interfacial bonding, resulting in flaws and decreased load transfer efficiency [24].

The optimal process parameter combination for maximal hardness, as shown by the main effect map, is a higher melting

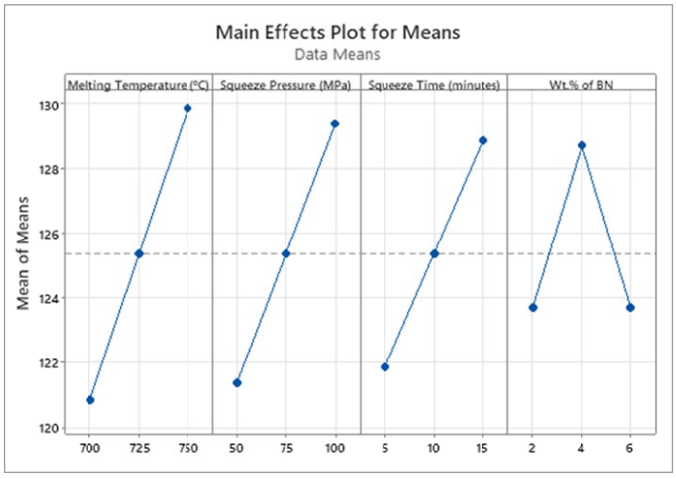

Fig. 2. Hardness of Main effect plot

TABLE 5

Input and response parameters for L9 OA under NaCl exposure

Squeeze Casting Specimen (SCS)	Melting Temperature (°C)	Squeeze Pressure (MPa)	Squeeze Time (minutes)	Wt.% of BN	Hardness VHN	UTS MPa
SCS1	700	50	5	2	111.7	253
SCS2	700	75	10	4	124.2	266
SC3	700	100	15	6	126.7	272.3
SCS4	725	50	10	6	119.7	261.8
SCS5	725	75	15	2	127.2	271.3
SCS6	725	100	5	4	129.2	270.8
SCS7	750	50	15	4	132.7	275.8
SCS8	750	75	5	6	124.7	266.3
SCS9	750	100	10	2	132.2	273.8

TABLE 6

Means for Hardness Response Table

Level	Temperature (Melting) (°C)	Squeeze Pressure (MPa)	Squeeze Time (minutes)	Wt.% of BN
1	120.9	121.4	121.9	123.7
2	125.4	125.4	125.4	**128.7**
3	**129.9**	**129.4**	**128.9**	123.7
Delta	9.0	8.0	7.0	5.0
Rank	1	2	3	4

temperature of 750°C, a 100 MPa higher squeeze pressure, a longer squeeze duration of 15 minutes, and a medium BN concentration of 4 wt.%. Higher melting temperatures increase material flow and reduce porosity, while greater squeezing pressure and duration improve densification and grain refinement, resulting in improved hardness. The 4 wt.% BN provides excellent reinforcement without significant particle agglomeration, which happens at 6 wt.% BN. This ensures superior load transmission and mechanical strength. TABLE 7 presents the hardness of ANOVA and it confirm the all chosen input pro-

TABLE 7

Hardness Analysis of Variance

Source	DF	Adj SS	Adj MS	F-Value	P-Value	Contribution %
Melting Temperature (ºC)	2	121.50	60.75	9.05	0.02	35.2
Squeeze Pressure (MPa)	2	96.00	48.00	7.9	0.035	27.8
Squeeze Time (minutes)	2	73.50	36.75	5.8	0.04	21.1
Wt.% of BN	2	50.00	25.00	4.9	0.045	14.4
Error	2	4.16	2.08			1.20
Total	8	345.16				100

cess parameters for optimization is having significant effect on hardness by verifying the *P* value of all parameters is less than 0.05 [25]. Contribution percentage of melting temperature, Squeeze pressure, squeeze time and wt.% of BN on hardness is 35.2%, 27.8%, 21.1% and 14.4% respectively.

3.1.2. Effect of input process parameters on UTS

TABLE 8 displays the response for means of UTS and it exhibit that influence sequence of input process parameters for squeeze casting is squeeze casting, squeeze pressure, melting temperature and wt.% of BN. The input process parameters which are optimized combination for UTS is higher of 750°C melting temperature, 100 MPa squeeze pressure, 15 minutes squeeze time and medium level of 4 wt.% of BN. Fig. 3 presents the UTS main effect plot.

TABLE 8

UTS Response Table for Means

Level	Melting Temperature (ºC)	Squeeze Pressure (MPa)	Squeeze Time (minutes)	Wt.% of BN
1	263.8	263.5	263.4	266.0
2	268.0	267.9	267.2	**270.9**
3	**272.0**	**272.3**	**273.1**	266.8
Delta	8.2	8.8	9.8	4.8
Rank	3	2	1	4

From the main effect plot, The UTS is increases with an increase in melting temperature from 700 to 750°C, pressure of squeeze from 50 to 100 MPa, and time of squeeze from 5 to 15 minutes is due to improved material densification, reduced porosity, and improved bonding between matrix and reinforcement, which leads to better load transfer. Higher melting temperatures improve fluidity, assisting in the uniform distribution of reinforcement, whilst greater squeezing pressure and duration promote finer microstructure and remove shrinkage flaws. Furthermore, increasing BN content from 2 to 4 wt.% strengthens the composite by refining grain structure and improving load-bearing capacity; however, at 6 wt.% BN, UTS decreases due to particle agglomeration and weakened interfacial bonding, which introduce stress concentrations and defects, reducing mechanical performance [26]. ANOVA for UTS is displayed in TABLE 9. The influence percentage of melting temperature, squeeze pressure, squeeze time and wt.% of BN on UTS is 24.7%, 28.5%, 35.9% and 10.1% respectively.

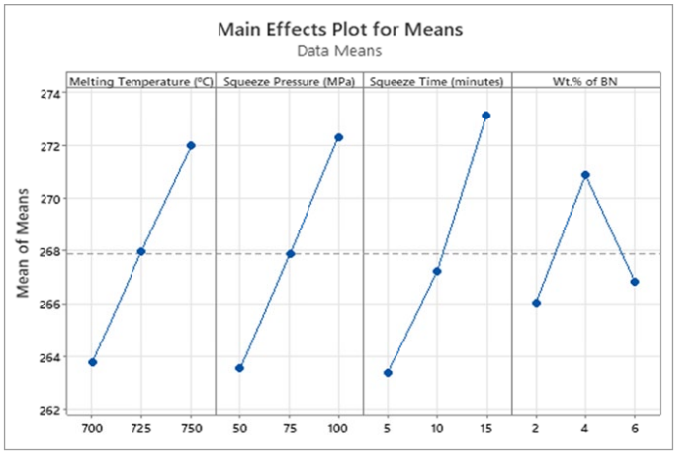

Fig. 3. UTS Main effect plot

3.1.4. Input process parameters optimization of squeeze casting on UTS and hardness by using GRA

Best combination of input process parameters for squeeze casting on hardness and UTS is analysed by using GRA. By em-

TABLE 9

UTS Analysis of Variance

Source	DF	Adj SS	Adj MS	F-Value	P-Value	Contribution %
Melting Temperature (ºC)	2	100.88	50.44	8.68	0.032	24.7
Squeeze Pressure (MPa)	2	115.29	57.64	9.05	0.03	28.5
Squeeze Time (minutes)	2	145.29	72.64	12.25	0.028	35.9
Wt.% of BN	2	40.49	20.24	4.2	0.04	10.1
Error	2	4.23	2.54	—	—	1.04
Total	10	404.17	—	—	—	—-

ploying GRA with the higher the better basis L9 OA based hardness and UTS responses were determined the normalized data, evaluation sequence, GRC and GRG. The higher value of normalized data, GRC and GRG represents the best blend of input process parameters. The lower value of evaluation sequence represents poor combination of input process parameters on responses. TABLE 10 displays the GRA result of optimization of squeeze casting process parameters on hardness and UTS. From the obtained results, L7 displays the higher GRG and hence L7 is ranked as 1 [27]. The obtained GRG is optimized by using the software Minitab 19. TABLE 11 presents the response for GRG and it is revealed that higher level of 750°C melting temperature, 100 MPa squeeze pressure, 15 minutes squeeze time and medium level of 4 wt.% of BN input parameter combination is optimum parameter combination for GRG.

TABLE10

GRA result of optimization of squeeze casting process parameters

Normalized value		Evaluation order		GRC		GRG	Rank
VHN	UTS	VHN	UTS	VHN	UTS		
0.000	0.000	1.000	1.000	0.333	0.333	0.3333	9
0.595	0.570	0.405	0.430	0.553	0.538	0.5452	7
0.714	0.846	0.286	0.154	0.636	0.765	0.7007	4
0.381	0.386	0.619	0.614	0.447	0.449	0.4478	8
0.738	0.803	0.262	0.197	0.656	0.717	0.6866	5
0.833	0.781	0.167	0.219	0.750	0.695	0.7226	3
1.000	1.000	0.000	0.000	1.000	1.000	1.0000	1
0.619	0.583	0.381	0.417	0.568	0.545	0.5565	6
0.976	0.912	0.024	0.088	0.955	0.851	0.9026	2

TABLE 11

Response Table for Means of GRG

Level	Melting Temperature (°C)	Squeeze Pressure (MPa)	Squeeze Time (minutes)	Wt.% of BN
1	0.5264	0.5937	0.5375	0.6409
2	0.6190	0.5961	0.6319	**0.7559**
3	**0.8197**	**0.7753**	**0.7958**	0.5684
Delta	0.2933	0.1816	0.2583	0.1876
Rank	1	4	2	3

Fig. 4 depicts the GRG main effect plot and it is revealed that increasing of melting temperature from 700 to 750, squeeze pressure from 50 to 100 MPa, squeeze time from 5 to 15 minutes increases the GRG and from wt.% of BN from 2 to 4 enhances and decreases by 6 wt.% [28]. TABLE 12 depicts the GRG ANOVA and it shows that all the process parameters of input are significant on GRG due to the p value of all input parameters is less than the 0.05. Influencing fraction of melting temperature, squeeze pressure, squeeze time and wt.% of BN on GRG is 37.1, 17.9,28.2 and 14.7% respectively.

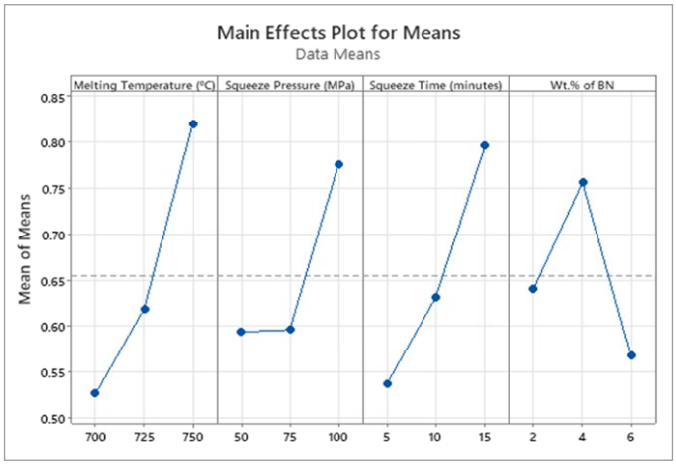

Fig. 4. Main effect plot for GRG

The best and optimum combination for input process parameters of squeeze casting on both Hardness and UTS is 750°C melting temperature, 100 MPa squeeze pressure, 15 minutes squeeze time and 4 wt.% of BN.

3.2. Metallurgical examination

The AA7075/12wt.%TiC/xwt.%BN (0, 2, 4 and 6) HMMCs were fabricated by the optimized squeeze casting process parameters and these composites were underwent to SEM and EDAX test to confirm the appearance of elements and microstructure.

Fig. 5(a-b) and TABLE 13 displays the EDAX test result for fabricated AA7075, AA7075 MMC and AA7075 HMMCs and it reveals the presence of Al and Zn in AA7075. Besides AA7075/12wt.%TiC has Al, Zn, Ti and C elements and also AA7075/12wt.%TiC/xwt.% of BN (2,4 and 6) has Al, Zn, Ti, C, B and N. The increasing of wt.% of BN enhances the wt.% of B and N elements in the fabricated AA7075 HMMCs [29].

TABLE 12

GRG Analysis of Variance

Source	DF	Adj SS	Adj MS	F-Value	P-Value	Contribution %
Melting Temperature (°C)	2	0.13489	0.06744	8.24	0.02	37.1
Squeeze Pressure (MPa)	2	0.06510	0.03255	4.32	0.035	17.9
Squeeze Time (minutes)	2	0.10250	0.05125	7.65	0.026	28.2
Wt.% of BN	2	0.05367	0.02684	3.98	0.041	14.7
Error	2	0.0072	0.0014			1.9
Total	10	0.36336				100

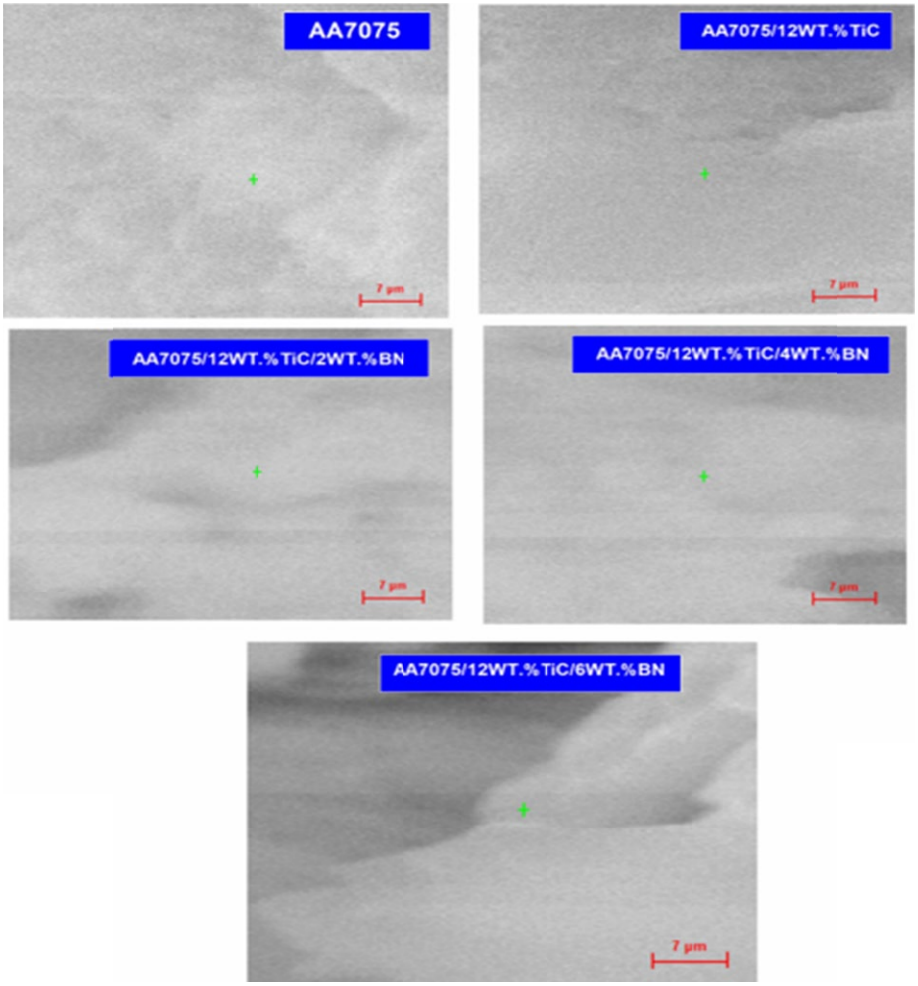

Fig. 5a. AA7075 and its composites SEM micrograph EDAX test result

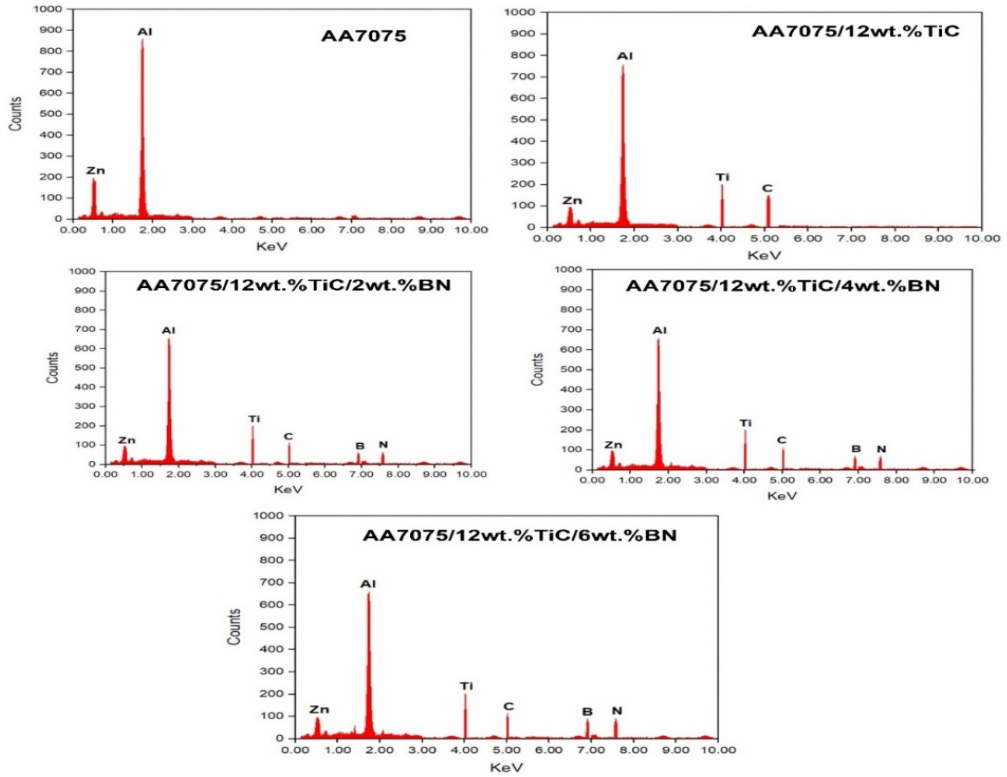

Fig. 5b. EDAX test result of AA7075 and its composites

TABLE 13

EDAX test results of AA7075 and its composites

Composite	Al	Zn	Ti	C	B	N
AA7075	78.329	4.928	—	—	—	—
AA7075/12wt.%TiC	76.549	4.816	9.646	2.407	—	—
AA7075/12wt.%TiC/2wt.%BN	74.768	4.704	9.645	2.407	0.871	1.129
AA7075/12wt.%TiC/4wt.%BN	72.988	4.592	9.643	2.407	1.742	2.258
AA7075/12wt.%TiC/6wt.%BN	71.207	4.480	9.642	2.407	2.614	3.386

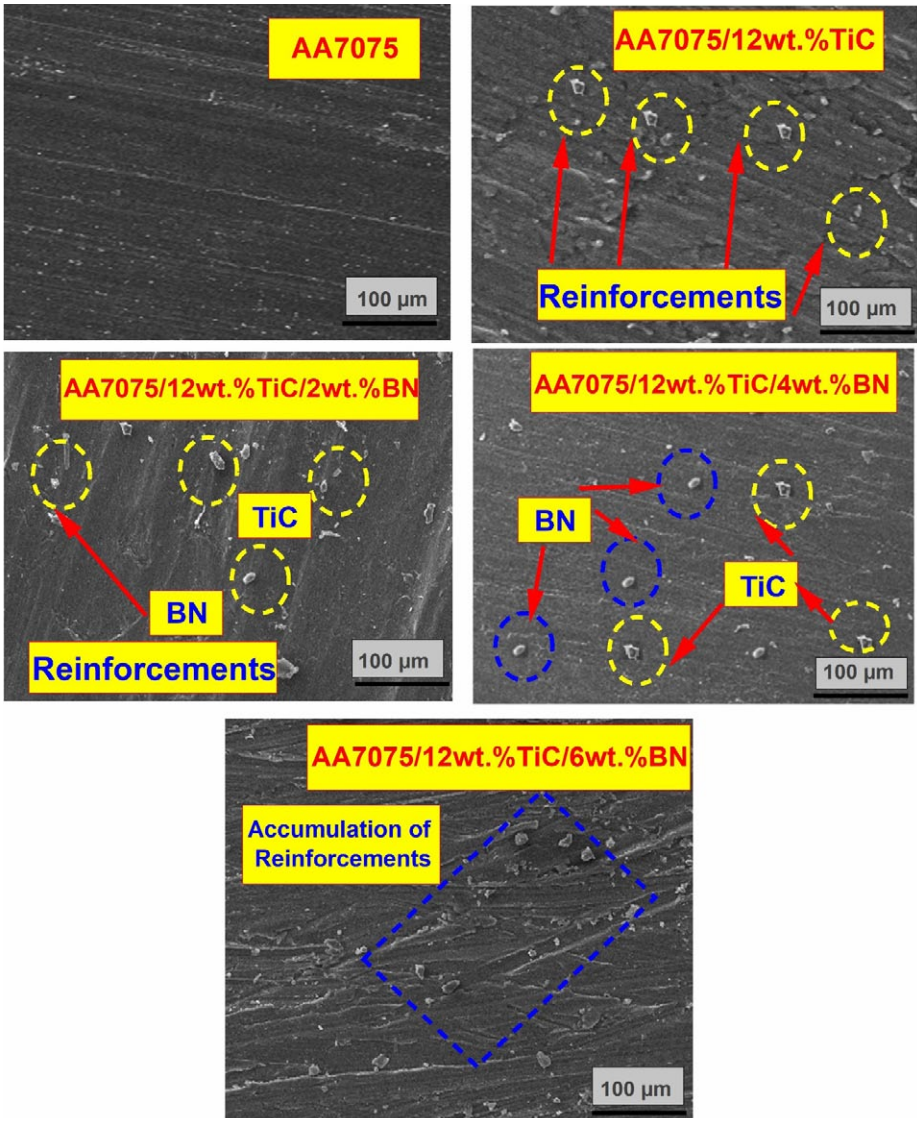

Fig.6. SEM image of AA7075 and its composites

The SEM test result for AA7075, AA7075/12wt.%TiC, A7075/12wt.%TiC/2wt.%BN, AA7075/12wt.%TiC/4wt.%BN and AA7075/12wt.%TiC/6wt.%BN is displayed in Fig. 6. The SEM image of AA7075 confirms that there is no presence of reinforcements and aa7075/12wt.%TiC exhibit that the presence of TiC in the matrix material AA7075. SEM image of AA7075/12wt.%TiC/xwt.% of BN (2,4 and 6) exhibit that adding of BN from 2 to 4 wt.% uniformly dispersed in the matrix AA7075.Adding of 6 wt.% causes the accumulation of BN in the AA7075/12wt.%TiC HMMCs. TiC and BN were differentiated by using particle shape of the reinforcements and confirmed through SEM image of TiC and BN powders [30].

3.3. Density and porosity examination

The density and porosity examination was carried out on A7075/wt.%TiC/wt.%BN HMMCs and the experimental results are depicted in the Fig. 7.

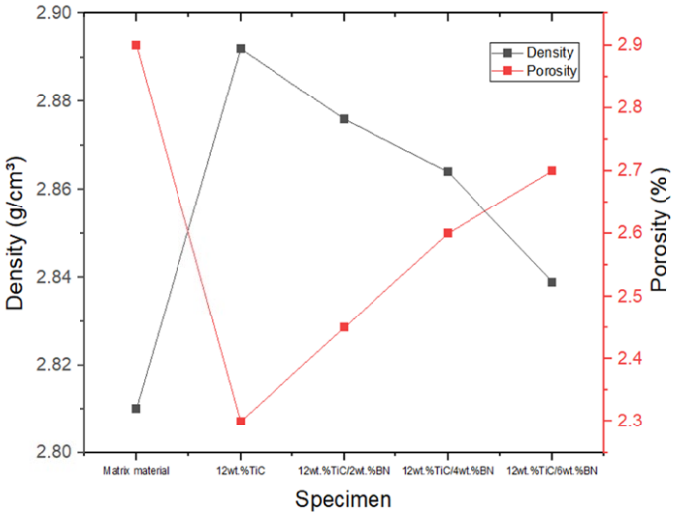

Fig. 7. Density and porosity plot of AA7075 and its composites

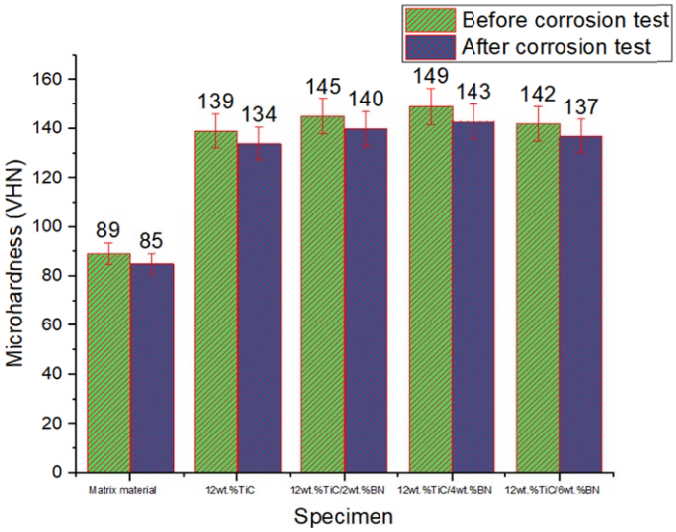

Fig. 8. Comparison of Microhardness results of AA7075 and its composites before and after corrosion

The results shows that, the density were increases from AA7075 to A7075/wt.%TiC MMCs and further it is decreased for additional reinforcement of wt.% of BN with A7075/wt.%TiC. The addition of wt.% of BN will slightly reduce the density meanwhile improves the strength, corrosion and metallurgical property of the AA7075 HMMCs. Similarly for porosity study shows that, the porosity were decreases from AA7075 and A7075/wt.% TiC MMCs and further it is increased for additional reinforcement of wt.% of BN with A7075/wt.%TiC. The addition wt.% of BN reduces the porosity which leads improve the mechanical property of AA7075 HMMCs. The optimized squeeze casted AA7075 HMMCs minimize the porosity and increase the density which would improve the overall performance of the material.

3.4. Microhardness examination

The Microhardness (VHN) of samples of AA7075, AA7075 MMC and AA7075 HMMCs was examined before and after the corrosion tests. The test samples are prepared as per the size of ASTM E384 the comparisons of the results of Microhardness test are shown in the Fig. 8.

This examination predicted the finest AA7075 HMMCs Composite which gives the highest Microhardness for both the samples of before and after the correction tests. From the study it is found that, the non-corroded AA7075/12wt.%TiC/4wt.%BN composite exhibit highest Microhardness of 149 VHN and similarly the corroded AA7075/12wt.%TiC/4wt.%BN composite exhibit highest Microhardness of 143 VHN. Also it is found that, adding higher or lower than the 4 wt.% of Boron Nitride in AA7075/12wt.%TiC decreases the Microhardess in both the non-corroded and corroded test samples. The 4 wt.% of Boron Nitride reduces the agglomeration in the AA7075 HMMCs Composite which improves the load transfer efficiency of the composite but the other than 4 wt.% of BN could reduce the load transfer efficiency.

3.5. Tensile strength examination

The Ultimate Tensile strength (UTS) of samples of AA7075, AA7075 MMC and AA7075 HMMCs was examined before and after the corrosion tests using Universal Testing Machine (UTM). The test samples are prepared as per the E-9 ASTM standard size and the prepare AA7075 HMMCs test samples are underwent of corrosion test. The comparisons of the results of UTS test are shown in the Fig. 9.

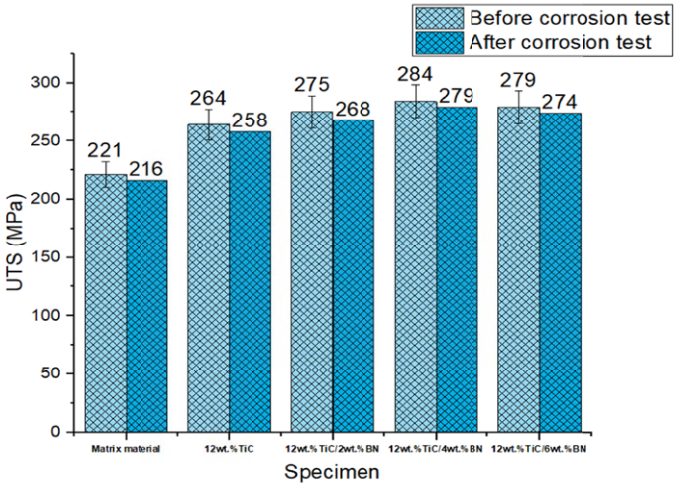

Fig. 9. Comparison of Ultimate Tensile strengths of AA7075 and its composites before and after corrosion

This examination predicted the finest AA7075 HMMCs Composite which gives the highest UTS for both the samples of before and after the correction tests. From the study it is found that, the non-corroded AA7075/12wt.%TiC/4wt.%BN composite exhibit highest Ultimate Tensile strength of 284 MPa and similarly the corroded AA7075/12wt.%TiC/4wt.%BN composite exhibit highest UTS of 279 MPa. Also it is found that, adding higher or lower than the 4 wt.% of Boron Nitride in

AA7075/12wt.%TiC decreases the Ultimate Tensile Strength in both the non-corroded and corroded test samples. The optimized AA7075/12wt.%TiC/4wt.%BN reinforcement of composite increase the strength of the materials, load transfer efficiency and corrosive resistant.

The surface fracture study was conducted in tensile test samples of AA7075/12wt.%TiC/xwt.% of BN (2, 4 and 6) and it is revealed in the Fig. 10. From this study it is revealed that, the AA7075 has higher porosity which leads to weaken the materials, AA7075/12wt.%TiC MMCs exhibit crack propagation which requires additional reinforcements, A7075/12wt.%TiC/2wt.%BN HMMCs exhibits ductile fracture and further reinforcement required to improve the ductile fracture and the optimized combination of AA7075/12wt.%TiC/4wt.%BN HMMCs shows the reduction of the ductile fracture, dimples and propagation of crack and improves the mechanical properties of the AA7075 HMMCs. The 6 wt.% BN additional reinforcement with AA7075/12wt.%TiC MMCs composites further initiates brittle fracture. These AA7075/12wt.%TiC/4wt.%BN HMMCs predominantly improves the fracture, strength for different load cases.

3.6. Compressive strength examination

The Compressive strength (CS) of AA7075, AA7075 MMC and AA7075 HMMCs were examined using Universal Testing Machine (UTM) before and after the corrosion tested samples. The test samples are prepared as per the E9 of ASTM standard size and the prepared AA7075 HMMCs test samples are undergo of corrosion test. The comparisons of the results of CS test are shown in the Fig. 11. This strength evaluation calculated the optimal AA7075 HMMCs Composite which gives the highest CS for both the samples of before and after

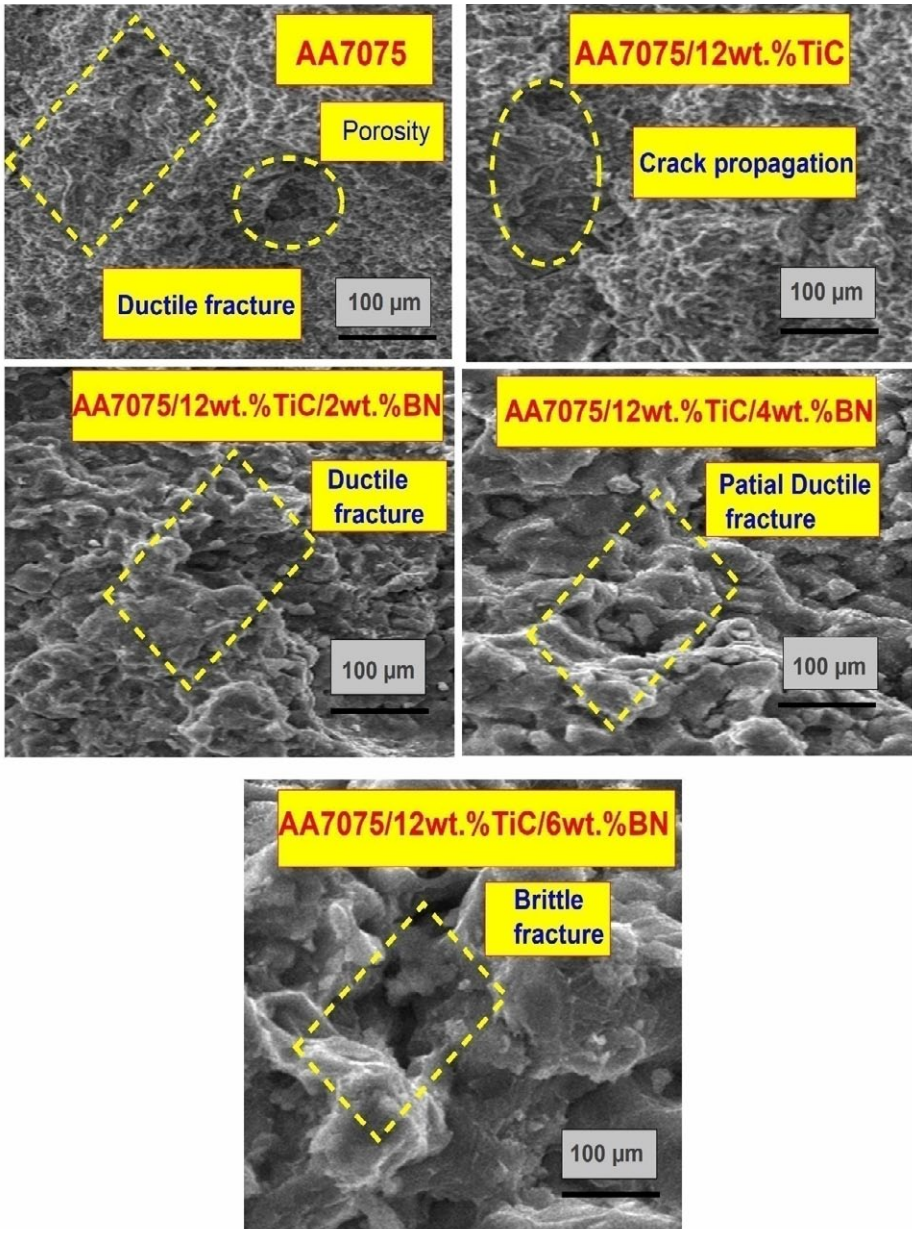

Fig. 10. Fracture surface of AA7075 and its composites

the correction tests. It is found from this CS study that, the non-corroded AA7075/12wt.%TiC/4wt.%BN composite exhibit highest Compressive strength of 296 MPa and similarly the corroded AA7075/12wt.%TiC/4wt.%BN composite exhibit highest Compressive Strength of 289 MPa. Also it is found that, the compressive strength is increases upto the AA7075/12wt.%TiC and 4 wt.% of Boron Nitride combination and CS is degreases beyond this combination of AA7075HMMCs in both the non-corroded and corroded test samples.

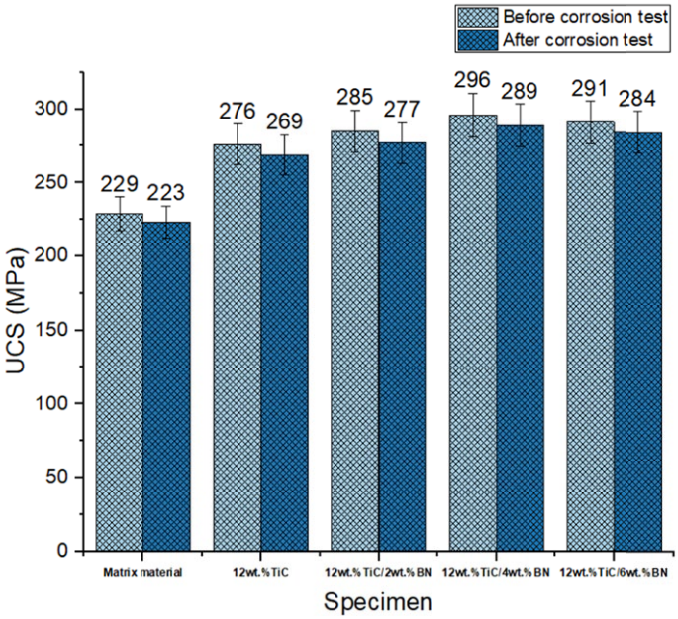

Fig. 11. Comparison of Compressive strengths of AA7075 and its composites before and after corrosion

3.7. Impact strength examination

The Impact Strength (IS) of AA7075 HMMCs was assessed experimentally as per the ASTM E23 standard. The Impact strength test sample was prepared as per the E23 size of ASTM standard and experimented the level of absorption of energy of different wt.% of sample prepared. The impact strengths ware tested for non-corroded and corroded impact specimens and the comparison of experimented results are shown in Fig. 12. The reinforcement of TiC and BN in AA7075 HMMCs is enhances the impact strength significantly than the non-reinforcement and non-corroded hybrid composite. It is observed that, the impact strength of the AA7075 HMMCs is improved for the addition of reinforcement upto AA7075/12wt.%TiC/4wt.%BN which is the optimal level of reinforcement of composite which enhances the impact strength due to finely distributed the TiC and BN. From the figure 12 it is observed that the maximum energy level of 17.9 J was achieved in AA7075/12wt.%TiC/4wt.%BN in non-corroded samples and similar for corroded samples 16.5 J maximum energy level was achieved in the same combination of AA7075 HMMCs. The maximum of 8.5% impact strength of improvement was enhanced by the non-corroded materials.

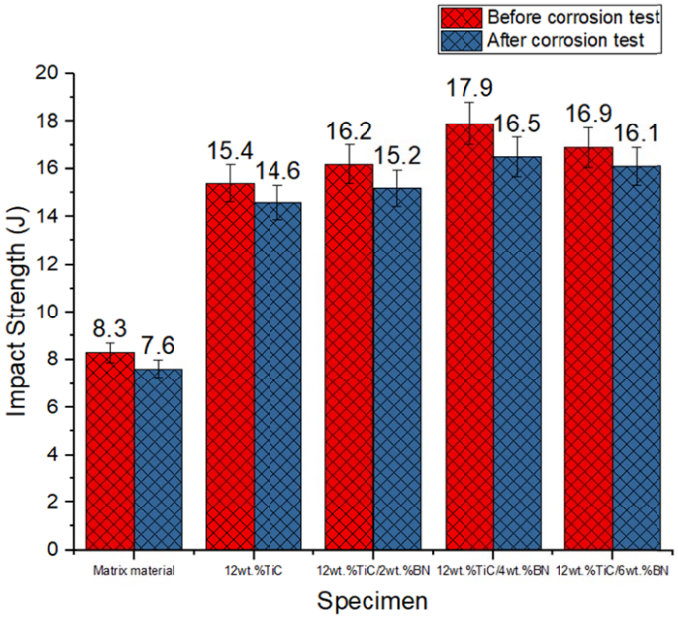

Fig. 12. Comparison of Impact strengths of AA7075 and its composites before and after corrosion

3.8. Tribology properties examination

Wear test was conducted on the fabricated AA7075 based composites with and without subjected to corrosion test at the condition of constant applied load of 30 N, constant sliding velocity 1.2 m/s and constant sliding distance 2000 m. Wear rate was calculated and the comparison of wear rate of AA7075 and its composites with and without subjecting to corrosion are shown in Fig. 13. Wear rate of AA7075 based composites subjected to corrosion test is higher than the wear rate of corrosion tested AA7075 based composites. From the wear test results, increasing of inclusion of wt.% of TiC and wt.% of BN enhances the wear resistance by reducing wear rate. The wear rate is reduced up to 4 wt.% of BN and slightly increased while adding 6 wt.% of BN.

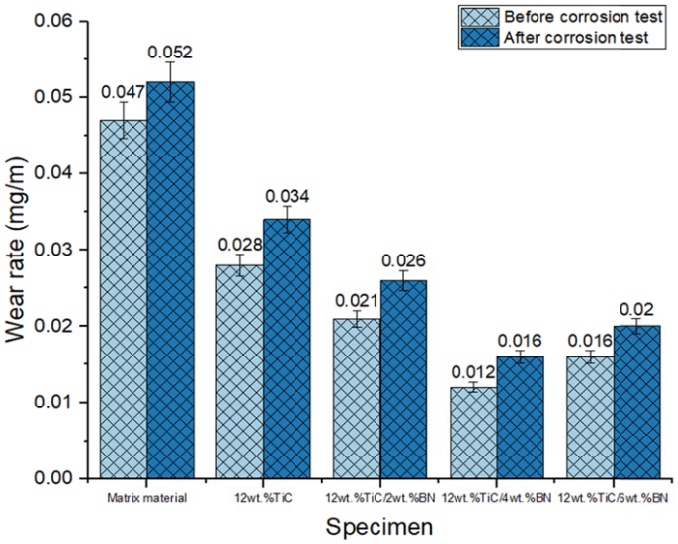

Fig. 13. Comparison of wear rate of AA7075 and its composites before and after corrosion

The graph compares wear rates for AA7075 matrix material and composites with different reinforcement mixes before and after corrosion testing. It is obvious that all specimens have a greater wear rate after corrosion than before corrosion. This shows that corrosion degrades the surface integrity by forming micro-cracks and pits, which then increases material loss during wear. Due to the lack of reinforcing phases, the matrix material (pure AA7075) has the greatest wear rates, both before (0.047 mg/m) and after corrosion (0.052 mg/m). The incorporation of 12 wt.% TiC greatly decreases the wear rate to 0.028 mg/m (before corrosion) and 0.034 mg/m (after corrosion), owing to the hardness of TiC particles. Furthermore, the addition of BN to TiC results in further improvement. For 12 wt.% TiC + 2 wt.% BN, the wear rate is 0.021 mg/m (before corrosion) and 0.026 mg/m (after corrosion). The highest wear resistance is shown with 12 wt.% TiC + 4 wt.% BN, with wear rates as low as 0.012 mg/m before corrosion and 0.016 mg/m after corrosion.

When the BN content is raised to 6 wt.%, the wear rate increases marginally to 0.016 mg/m (pre-corrosion) and 0.020 mg/m (after corrosion). This modest loss in performance is due to probable agglomeration of BN particles and reduction in matrix bonding strength, resulting in particle pull-out and micro-crack development during wear. The overall failure mechanism consists of corrosion-assisted wear, in which surface deterioration from corrosion serves as fracture starting sites, and abrasive and adhesive wear, in which hard TiC particles resist cutting and BN particles reduce friction. At a greater BN concentration (6 wt.%), particle clustering and weak bonding lead to localized material loss, somewhat decreasing the composite's wear resistance.

Fig. 14 displays the comparison of CoF of wear tested AA7075 and its composites before and after corrosion test. From the obtained results, adding of 12 wt.% of TiC and increasing of wt.% of BN from 2 to 4 reduces the CoF and adding of 6 wt.% of CoF slightly increases CoF. Besides, CoF of corrosion tested AA7075 and its composites are higher than CoF of non-corrosion tested AA7075 and its composites. The graph depicts the variation in coefficient of friction (CoF) for AA7075 matrix material and composites supplemented with TiC and BN, both before and after corrosion testing. All specimens' CoFs rise somewhat following corrosion, demonstrating that corrosion-induced surface deterioration promotes greater friction during sliding. The matrix material (AA7075) has the highest CoF values, with 0.274 before corrosion and 0.277 after corrosion, due to its relatively soft surface and absence of reinforcing phases to resist friction.

The addition of 12 wt.% TiC results in a considerable drop in CoF (0.214 before corrosion and 0.219 after corrosion), which is attributable to TiC particles' high hardness, which resists plastic deformation and reduces surface roughness during sliding. The inclusion of BN results in further improvements. The CoF decreases further to 0.198 (before corrosion) and 0.204 (after corrosion) with 12 wt.% TiC + 2 wt.% BN, but 12 wt.% TiC + 4 wt.% BN has the lowest CoF values. This phenomenon is explained by the solid lubricating feature of BN, which efficiently minimizes shear pressures at the sliding surface, resulting in decreased friction. However, after 6 wt.% BN addition, a modest rise in CoF is seen (0.187 before corrosion and 0.195 after corrosion). The increase is most likely due to the agglomeration of BN particles at larger concentrations, which might generate localized roughness and impair the homogeneous distribution of reinforcements, marginally elevating friction during sliding.

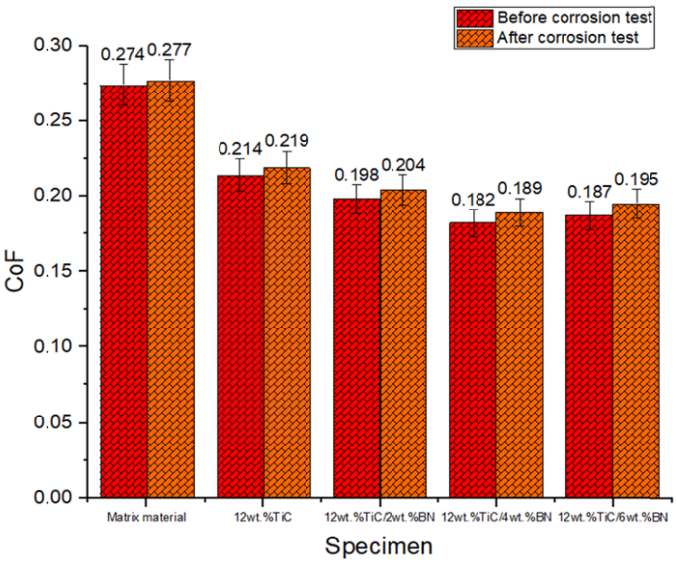

Fig. 14. Comparison of CoF AA7075 and its composites before and after corrosion

The failure mechanism that underpins these data is essentially a mix of corrosion-induced surface roughening and micro-crack development in the matrix following corrosion, which results in higher frictional resistance while sliding. Wear in non-corroded samples is primarily regulated by TiC particles' abrasion resistance and the lubricating effect of BN. However, following corrosion, the damaged and roughened surfaces encourage stronger mechanical interlocking and plowing, leading in a larger CoF than the non-corroded condition. Fig. 15 displays the worn surface of AA7075 and its composites after subjecting to corrosion test. Pits are formed on the surface of corrosion and wear tested AA7075. Wear tracks are formed on the surface of 12 wt.% TiC reinforced AA7075 based composites. Tribo film is formed on the surface of AA7075/12wt.%TiC/4wt.%BN composites. Narrow pits and wear tracs are formed on the surface of AA7075/12wt.%TiC/6wt.%BN composites due to accumulation of reinforcements.

Fig. 16 displays the wear debris of wear tested AA7075 and its composites after subjecting to corrosion test. The SEM micrographs of the collected wear debris show a clear development in particle shape as the composite formulation develops. Unreinforced AA7075 produces enormous, thin "flake-like" pieces, indicating delamination wear, as subsurface shear forces peel off layers of the ductile aluminum matrix. When 12 wt.% TiC is introduced, the flakes become smaller and more fractured as the hard TiC particles prevent crack growth and restrict the size of delaminated chips. Adding 2 wt.% and 4 wt.% BN to TiC transforms debris into finer, angular micro-chips. The TiC hardness resists plastic flow, while the BN's solid-lubricant ac-

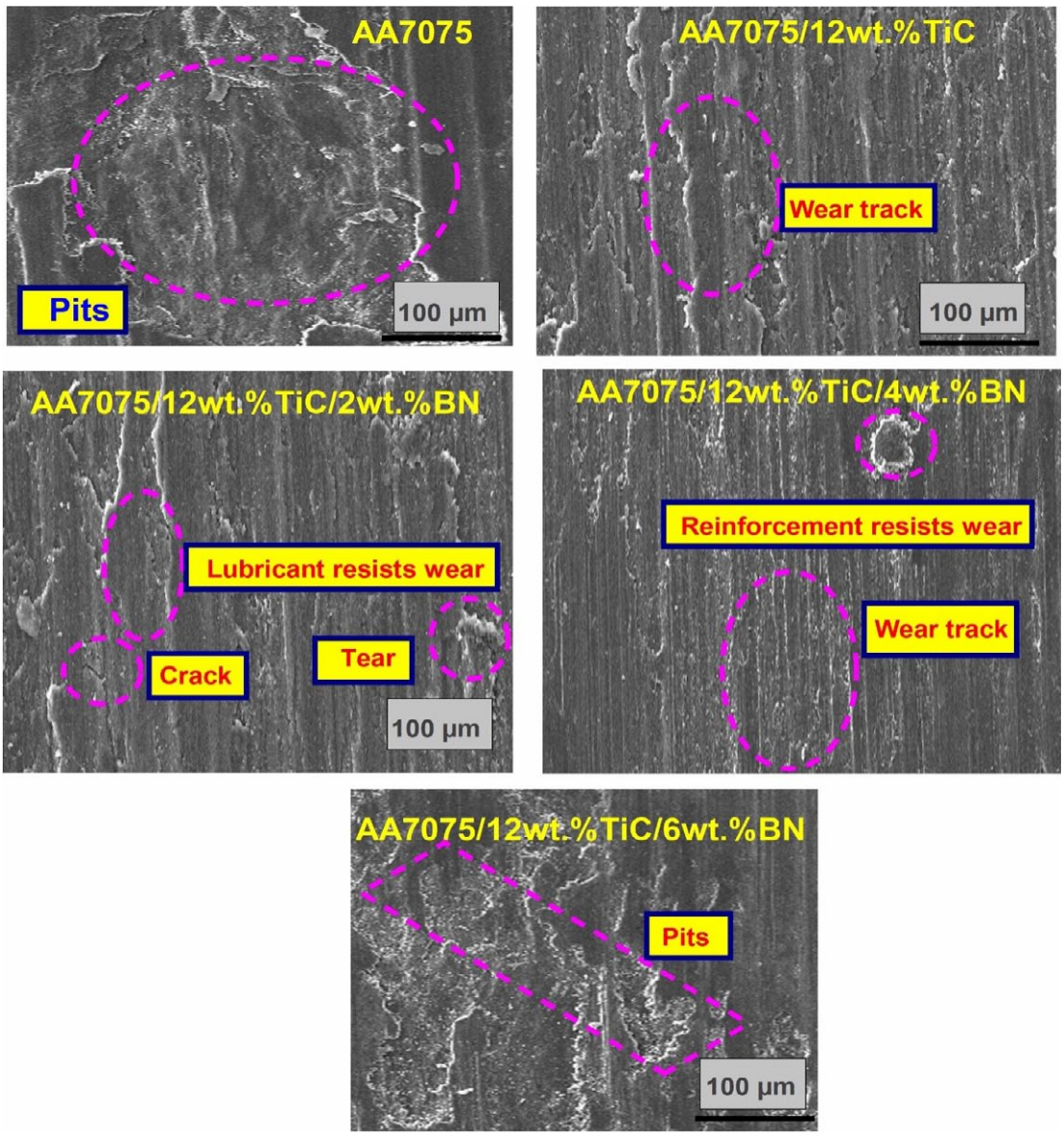

Fig. 15. Worn surface of AA7075 and its composites

tion reduces friction and shifts the dominant mechanism from large-scale delamination to abrasive micro-cutting. At 6% BN, worn pieces look folded and lamellar, indicating fatigue spallation. Excess BN is prone to agglomerate and form localized stress raisers that facilitate recurrent fracture nucleation under cyclic contact, resulting in tiny, coiled fatigue flakes rather than clean abrasive chips. The debris morphology evolves from unreinforced to TiC, TiC+BN, and TiC+high-BN, indicating a shift from delamination to fatigue-driven wear.

3.9. Corrosion property examination

The Salt Spray Corrosion Test was conducted at the condition of 120-hour spray application conducted at a pressure of 1.2 kg/cm^2, using a solution with a pH level of 8.2 on the fabricated AA7075, AA7075/12wt.%TiC and AA7075/12wt.%TiC/xwt.%BN (2,4 and 6) composites. Mass loss was calculated by measuring weight before and after corrosion test. Fig. 17 displays the comparison of corrosion rate of AA7075 and its composites. The adding of wt.% of TiC and inclusion of wt.% of BN from 2 to 4 reduces the corrosion rate and adding of 6 wt.% of BN increases the corrosion rate. The unreinforced AA7075 alloy has the highest corrosion rate, which decreases significantly with the addition of 12 wt.% TiC and further decreases as BN content increases from 2 to 4 wt.%, according to mass loss measurements. TiC particles, in particular, operate as inert, insoluble barriers, breaking up the continuous metal matrix and reducing the effective surface area accessible for chloride attack. Co-dispersion of 2-4 wt.% BN platelets densifies the composite by filling microchannels and reinforcing the adhering corrosion product layer. This prevents ion ingress and anodic dissolution. At 6 wt.% BN, the corrosion rate slightly increases due to BN agglomeration, which creates interfacial voids and micro-crevices for chloride accumulation and galvanic coupling. This leads to pitting and increased mass loss.

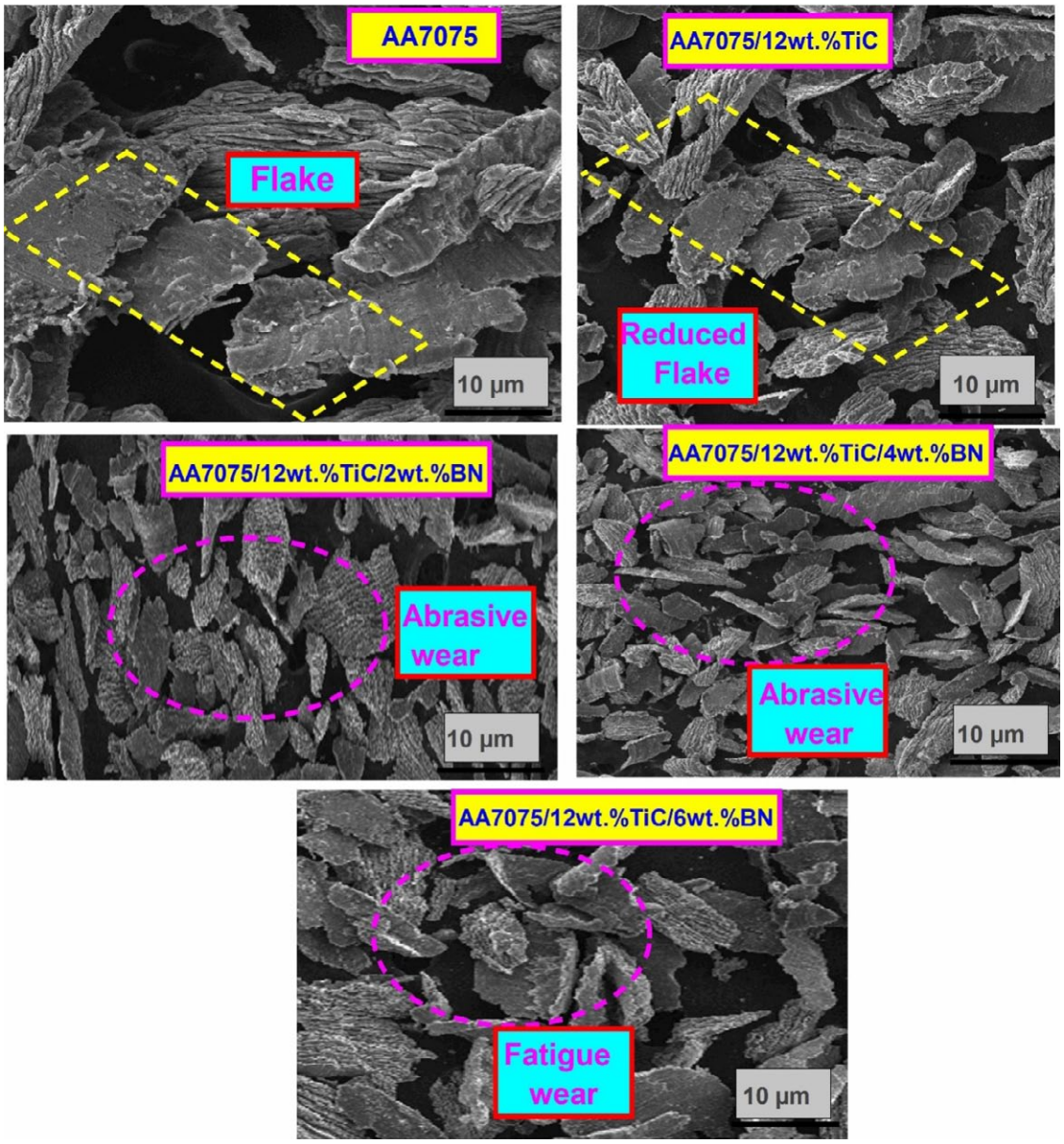

Fig. 16. Wear debris of AA7075 and its composites

The corrosion rate curve shows a gradual drop in salt-spray attack with reinforcements, followed by a tiny increase at the greatest BN loading. The AA7075 alloy corrodes at the fastest rate (0.782 mm/year). Adding 12 wt.% TiC reduces the rate by nearly half (0.483 mm^{-1}), as the hard, chemically inert TiC particles disrupt the continuity of the aluminum matrix and decrease the exposed anodic surface. Co-reinforcing with 2 wt.% and 4 wt.% BN reduces corrosion rate to 0.345 mm^{-1} and 0.277 mm^{-1}, respectively. The plate-like BN flakes fill micro-voids and promote a more adherent, compact corrosion-product layer, preventing chloride ingress and slowing metal dissolution. When BN is raised to 6 wt.%, the corrosion rate returns to 0.297 mm yr^{-1}. This is likely owing to BN agglomeration and the creation of interfacial gaps that function as small cathodic sites or fissures, enabling pitting and slightly accelerating mass loss.

Fig. 17 display the SEM image of corroded surface of AA7075 and its composites. SEM micrographs of corroded

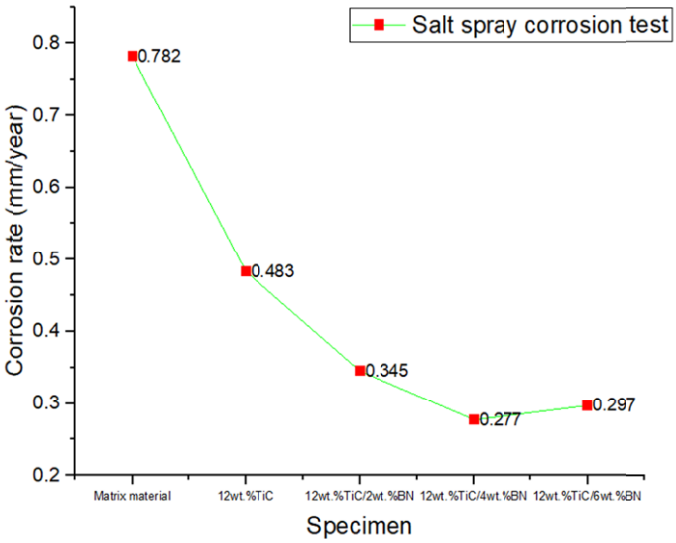

Fig. 17. Corrosion rate of AA7075 and its composites

surfaces reflect mass-loss rates and show how TiC and BN reinforcements affect corrosion morphology. The unreinforced AA7075 (top left) reveals a significantly deteriorated surface covered by thick, porous corrosion products and large fissures, commensurate with its greatest corrosion rate (0.782 mm^{-1}/yr). In the 12 wt.% TiC composite (top right), the surface is more evenly coated by a thin, adherent oxide layer that seems to anchor on the hard TiC particles. This enhanced barrier coincides with an approximately 40% decline in corrosion rate (0.483 mm yr^{-1}).

Adding 2 wt.% BN (bottom left) refines the surface, leaving only sparse, shallow pits. BN platelets block micro-channels in the matrix and maintain a tighter corrosion-product layer, providing a corrosion rate of 0.345 mm yr^{-1}. At 4 wt.% BN (bottom center), the surface is nearly pit-free and smooth, showing that the TiC/BN network effectively limits chloride entry and decreases anodic dissolution – this specimen displays the lowest corrosion rate (0.277 mm/year). At 6 wt.% BN (bottom right), the SEM shows localized oxide nodules and tiny pits surrounding apparent BN agglomerates, indicating interfacial voids that function as micro-crevice sites. This defect production explains the minor recovery in corrosion rate to 0.297 mm/yr^{-1}.

4. Conclusions

AA7075 and its composites reinforced by TiC and BN with 12 and 2,4 and 6 wt.% were fabricated by squeeze casting technique by using GRA optimized squeeze casting process parameters such as 750°C melting temperature, 100 MPa squeeze pressure, 15 minutes squeeze time. Contribution percentage of

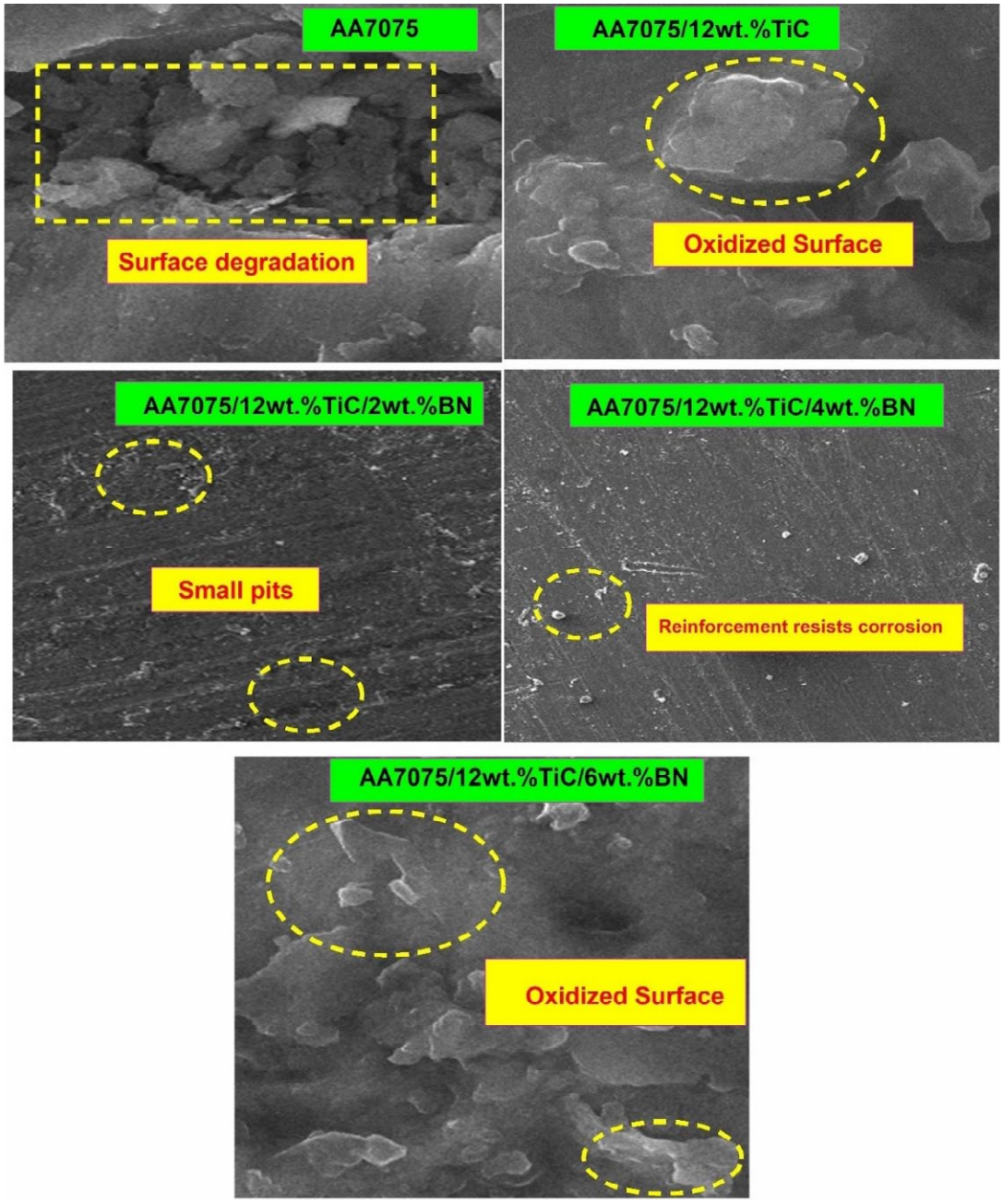

Fig. 18. Corroded surface of AA7075 and its composites

melting temperature, Squeeze pressure, squeeze time and wt.% of BN on hardness is 35.2%, 27.8%, 21.1% and 14.4% respectively. The input process parameters optimized combination for UTS is higher level of 750°C melting temperature, 100 MPa squeeze pressure, 15 minutes squeeze time and medium level of 4 wt.% of BN. Fig. 3 depicts the main effect plot for UTS. Contribution percentage of melting temperature, squeeze pressure, squeeze time and wt.% of BN on GRG is 37.1, 17.9,28.2 and 14.7% respectively. EDAX analysis verifies the presence of Al and Zn in the AA7075 matrix, as well as the effective integration of Ti, C, B, and N components into composites reinforced with TiC and BN. The strength of Ti, C, B, and N peaks rises with greater BN concentration, indicating successful reinforcement dispersion. SEM photos demonstrate the lack of reinforcements in AA7075 and the presence of TiC in AA7075/12wt.%TiC composites, with BN particles evenly distributed at 2-4 wt.% and agglomerated at 6 wt.%. TiC and BN were identified by their particle morphologies, as validated by SEM photographs of the powders. The addition wt.% of BN reduces the porosity which leads improve the mechanical property of AA7075 HMMCs. The addition of TiC and BN reinforcements to AA7075 greatly boosts its microhardness when compared to the unreinforced matrix. Even after corrosion testing, the composites retain greater microhardness values, with AA7075/12 wt.% TiC/4 wt.% BN providing the greatest performance. The non-corroded AA7075/12wt.%TiC/4wt.%BN composite exhibit highest Ultimate Tensile strength of 284 MPa and similarly the corroded AA7075/12wt.%TiC/4wt.%BN composite exhibit highest UTS of 279 MPa. The non-corroded AA7075/12wt.%TiC/4wt.%BN composite exhibit highest Compressive strength of 296 MPa and similarly the corroded AA7075/12wt.%TiC/4wt.%BN composite exhibit highest Compressive Strength of 289 MPa. Maximum energy level of 17.9 J was achieved in AA7075/12wt.%TiC/4wt.%BN in non-corroded samples and similar for corroded samples 16.5 J maximum energy level was achieved in the same combination of AA7075 HMMCs. The maximum of 8.5% impact strength of improvement was enhanced by the non-corroded materials. From the wear test results, increasing of inclusion of wt.% of TiC and wt.% of BN enhances the wear resistance by reducing wear rate. The wear rate is reduced up to 4 wt.% of BN and slightly increased while adding 6 wt.% of BN. The CoF decreases further to 0.198 (before corrosion) and 0.204 (after corrosion) with 12 wt.% TiC + 2 wt.% BN, but 12 wt.% TiC + 4 wt.% BN has the lowest CoF values. At 2 wt.% BN, surface pits are minimal due to BN blocking micro-channels, reducing corrosion to 0.345 mm/yr. At 4 wt.% BN, the surface is nearly pit-free, achieving the lowest corrosion rate of 0.277 mm/yr. At 6 wt. % BN, BN agglomerates cause micro-crevices, slightly increasing corrosion to 0.297 mm/yr.

REFERENCES

[1] S.A.A. Alem, M.H. Sabzvand, P. Govahi, P. Poormehrabi, M.H. Azar, S.S. Siouki, R. Rashidi, S. Angizi, S. Bagherifard, Advancing the next generation of high-performance metal matrix composites through metal particle reinforcement. Adv. Compos. Hybrid Mater. **8**, 1 (2024).
DOI: https://doi.org/10.1007/s42114-024-01057-4

[2] S. Singh, A. Gupta, V.S. Sharma, R. Harichandran, Production and high temperature wear characterization of AA 7075/Al2O3/Graphite hybrid nanocomposites by enhanced stir and ultrasound assisted casting method. Mater. Res. Express **6**, 12, 125072 (2019).
DOI: https://doi.org/10.1088/2053-1591/ab5aa1

[3] M. Ponnusamy, Ashok Raj Rajendran, A.P. Dhanaraj, P.S. Karuppiah, Experimental study of scandium addition and precipitate formation on the mechanical and tribological properties of Ultrasonic-assisted stir-cast AA7075 hybrid metal matrix composites. Matéria **30** (2025).
DOI: https://doi.org/10.1590/1517-7076-rmat-2024-0694

[4] S. Jeyaprakasam, M. Gnanasekaran, S. Magibalan, R.P. Singh, V. Mohanavel, S. Kannan, J. Giri, M.S. Ali, P. Barmavatu, Tribological, Mechanical and microstructure characteristics of hybrid aluminium matrix composite containing titanium carbide (TiC) and graphite particles. J. Mater. Res. Technol. (2024).
DOI: https://doi.org/10.1016/j.jmrt.2024.10.167

[5] H. Ahmadian, T. Zhou, A. Alansari, A. S. Kumar, A. Fathy, M. Elmahdy, Q. Yu, G. Weijia, Microstructure, mechanical properties and wear behavior of Mg matrix composites reinforced with Ti and nano SiC particles. J. Mater. Res. Technol **31**, 4088-4103 (2024). DOI: https://doi.org/10.1016/j.jmrt.2024.07.125

[6] A. Jamali, S.E. Mirsalehi, Production of AA7075/ZrO2 nanocomposite using friction stir processing: Metallurgical structure, mechanical properties and wear behavior,. CIRP J. Manuf. Sci. Technol. **37**, 55-69 (2022).
DOI: https://doi.org/10.1016/j.cirpj.2021.12.008

[7] R.R. Kumar, M. Ravichandran, S.V. Alagarsamy, Synthesis, mechanical and tribological behaviours of boron nitride reinforced AA7075 composites produced by stir casting technique. Surf. Topogr. Metrol. Prop. **12**, 2, 025022 (2024).
DOI: https://doi.org/10.1088/2051-672X/ad4fa8

[8] S.S. Kumar, G. Karthikeyan, K. Panneer Selvam, Optimization on EDM process parameters of AA 8011 based hybrid Metal Matrix composites. J. Phys. Conf. Ser. **2925**, 1, 012015 (2024).
DOI: https://doi.org/10.1088/2051-672X/ad4fa8

[9] S.S. Kumar, G. Karthikeyan, K. Panneer Selvam, Optimization of Squeeze Casting Process Parameters on AA8011 Based Hmmcs Under NaCl Environment. Arch. Metall. Mater **69**, 3, 1047-1060 (2024). DOI: https://doi.org/10.24425/amm.2024.150925

[10] M. Zhang, W.-W. Zhang, H.-D. Zhao, D.-T. Zhang, Y.-Y. Li, Effect of pressure on microstructures and mechanical properties of Al-Cu-based alloy prepared by squeeze casting. Transactions of Nonferrous Metals Society of China **17**, 3, 496-501 (2007).

[11] R. Bertolini, E. Simonetto, L. Pezzato, A. Fabrizi, A. Ghiotti, S. Bruschi, Mechanical and corrosion resistance properties of AA7075-T6 sub-zero formed sheets. The Int. J. Adv. Manuf. Technol. **115**, 9-10, 2801-2824 (2021).
DOI: https://doi.org/10.1007/s00170-021-07333-7

[12] O.J. Akinribide, O.D. Ogundare, S.O. Akinwamide, F. Gamaoun, P.A. Olubambi, Alloying effect of copper in AA-7075 aluminum

composite using bale out furnace. J. Mater. Res. Technol. **18**, 3849-3856 (2022).
DOI: https://doi.org/10.1016/j.jmrt.2022.04.054

[13] X. Li, H. Das, M. Pole, L. Li, A. Soulami, G.J. Grant, D.R. Herling, M. Efe, Exceptional strength and wear resistance in an AA7075/TiB2 composite fabricated via friction consolidation. Mater. Des. **242**, 113006 (2024).
DOI: https://doi.org/10.1016/j.matdes.2024.113006

[14] S.P. Dwivedi, V. Chaudhary, S. Sharma, A. Pattanaik, P.V. Kumar, Y.S. Bisht, V. Singh, M. Abbas, D. Kozak, J. Lozanovic, A. Kumar, Synthesis and Purification of Nano-sized Titanium Carbide Particles through Vacuum Carbothermal Reduction for enhanced Mechanical, Microstructural Morphology, and Tribological Properties in Friction Stir Processed A356-based Aluminum Composites. J. Mater. Res. Technol. (2024).
DOI: https://doi.org/10.1016/j.jmrt.2024.10.199

[15] J. Chen, J. Chen, S. Wang, Q. Sun, J. Cheng, Y. Yu, J. Yang, Tribological properties of h-BN matrix solid-lubricating composites under elevated temperatures. Tribol. Int. **148**, 106333 (2020).
DOI: https://doi.org/10.1016/j.triboint.2020.106333.

[16] H.M. Sabbar, Z. Leman, S.B. Shamsudin, S.M. Tahir, C.N.A. Jaafar, M.A.A. Hanim, Z.N. Ismsrrubie, S. Al-Alimi, AA7075-ZRO2 Nanocomposites produced by the consecutive Solid-State Process: A Review of Characterisation and Potential Applications. Metals **11**, 5, 805 (2021).
DOI: https://doi.org/10.3390/met11050805

[17] H. Jamshaid, A.A. Khan, R.K. Mishra, N. Ahmad, V. Chandan, V. Kolář, M. Müller, Taguchi grey relational analysis (GRA) based multi response optimization of flammability, comfort and mechanical properties in station suits. Heliyon **11**, 4, e42508 (2025). DOI: https://doi.org/10.1016/j.heliyon.2025.e42508

[18] A. Gnanavelbabu, K.T.S. Surendran, S. Kumar, Process optimization and studies on mechanical characteristics of AA2014/AL2O3 nanocomposites fabricated through ultrasonication assisted Stir–Squeeze casting. Int. J. Metalcast **16**, 2, 759-782 (2021).
DOI: https://doi.org/10.1007/s40962-021-00634-3

[19] Ashok Raj Rajendran, P. Mathiyalagan, B. Kumaragurubaran, M.G. Skanda, V. Sivaganesan, A.S. Prakash, K. Panneer Selvam, Optimization of wear parameters of aluminium 7075 hybrid composites using taguchi technique. J. Phys. Conf. Ser. **2925**, 1, 012016 (2024).
DOI: https://doi.org/10.1088/1742-6596/2925/1/012016

[20] R. Ashok Raj R, A. Santhosh Prakash, D. Antony Prabu, S. Vijayan, Optimization on hardening process parameters of alumnium alloy 7075 based composites using gra approach. Mater. Res. Express **10**, 10, 105007 (2023).
DOI: https://doi.org/10.1088/2053-1591/ad019e

[21] P. Rajendran, V. Duraisamy, A.R. Rajendran, R.V. Loganathan, Optimization on the electrical discharge machining (EDM) process parameters of aged AA7075/TiC metal matrix composites. Rev. Metal. **59**, 3, e245 (2023).
DOI: https://doi.org/10.3989/revmetalm.245

[22] N. Murugan, K.S. Jayakumar, R. Ashok Raj, D. Antony Prabu, Enhanced mechanical and tribological properties of ultrasonically assisted stir-cast AA7075 metal matrix composites in challenging corrosive environments. Mater. Res. Express **11**, 8, 086502 (2024).
DOI: https://doi.org/10.1088/2053-1591/ad674d

[23] Nikhilesh Singh, Deepika Deepika, Tribological properties of novel Al 7075(T6)-SiC-crumb rubber-MoS2-based hybrid composites: An experimental approach towards green revolution. Proc. Inst. Mech. Eng., Part L: J. Mater.: Des. Appl. **238**, 759-782(2023).
DOI: https://doi.org/10.1177/14644207231168

[24] A.A. Akinwande, A.A. Adediran, O.A. Balogun, M.E. Yibowei, A.A. Barnabas, H.K. Talabi, B.J. Olorunfemi, Optimization of selected casting parameters on the mechanical behaviour of Al 6061/glass powder composites. Heliyon **8**, 5, e09350 (2022).
DOI: https://doi.org/10.1016/j.heliyon.2022.e09350

[25] B.N.A. Deep, S. Rajanna, K.N. Krishnamurthy, G.C.M. Patel, T. Ganesha, G.V.G. Reddy, M. Hasan, E. Linul, Ultrasonic assisted stir squeeze casting of AA5456/Al2O3-SiC-Gr-MoS2 hybrid nanocomposites: Microstructure and strengthening analysis. J. Mater. Res. Technol. **34**, 1611-1635 (2025).
DOI: https://doi.org/10.1016/j.jmrt.2024.12.172

[26] A. Ramezani, H.J. Aval, R. Jamaati, Influence of Al2O3 addition on microstructure, mechanical strength, and wear behavior of AA7075- Al2O3 matrix composites fabricated using deformation-driven metallurgy. Results Eng. **26**, 104714 (2025).
DOI: https://doi.org/https://doi.org/10.1016/j.rineng.2025.104714

[27] A. Kumar, V. Kumar, Fabrication and optimization of AA7075-7%SiC surface composites using RSM technique via friction stir processing. Journal of Alloys and Metallurgical Systems **3**, 100022 (2023). DOI: https://doi.org/10.1016/j.jalmes.2023.100022

[28] S. Vijayakumar, P.S.S. Kumar, P.S. Kumar, S. Manickam, G.B. Ramaiah, H.P. Pydi, The effect of Stir-Squeeze casting process parameters on mechanical property and density of aluminum matrix composite. Adv. Mater. Sci. Eng. 1-10 (2022).
DOI: https://doi.org/10.1155/2022/3741718

[29] A. Canakci, T. Varol, Microstructure and properties of AA7075/Al–SiC composites fabricated using powder metallurgy and hot pressing. Powder Technol **268**, 72-79 (2014).
DOI: https://doi.org/10.1016/j.powtec.2014.08.016

[30] C. Potisawang, S. Talangkun, K. Ponhan, Improvement of microstructure and mechanical properties for Al7075 aluminium reinforced with hybrid graphite and SiC particles via a combination of mechanical alloying and stir casting. Mater. Res. Express **12**, 016509 (2025).
DOI: https://doi.org/10.1088/2053-1591/ada5b8